2015 IEEE International Conference on Robotics and Automation (ICRA)
Washington State Convention Center
Seattle, Washington, May 26-30, 2015

Variable-speed Quadrupedal Bounding Using Impulse Planning: Untethered High-speed 3D Running of MIT Cheetah 2

Hae-Won Park[1], Sangin Park[1], and Sangbae Kim[1]

Abstract— **This paper introduces a bounding gait control algorithm that allows a variable-speed running in the MIT Cheetah 2. A simple impulse planning algorithm is proposed to design vertical and horizontal force profiles which make net impulse on the system during one cycle zero. This design of force profiles leads to the conservation of linear momentum over a complete step, providing periodicity in horizontal and vertical velocity. When designed profiles are applied to the system, periodic orbits with an ability to change running speed are obtained. A virtual compliance control in the horizontal and vertical direction has been added onto the designed force profiles to stabilize the periodic orbits. The experimental results show that the algorithm successfully achieved untethered 3D running of the MIT Cheetah 2, with speeds ranging from 0 m/sec to 4.5 m/sec on treadmills as well as on grassy fields.**

I. INTRODUCTION

Quadrupedal animals exhibit a remarkable capability to achieve high-speed, agile, and robust locomotion. Recent advances in the study of quadrupedal robots have shown a potential to realize this great locomotion capability in robotic systems. BigDog [1], LS3 and WildCat [2] developed by Boston Dynamics have demonstrated dynamic walking and fast running in outdoor environments with great robustness. Trotting gaits shown by StarlETH [3] and HyQ [4] are other exemplary results of advances in quadrupedal robotic systems. Recently, MIT Cheetah 1 and 2, research platforms with a unique electric actuation system for the study of high-speed quadrupedal locomotion [5], [6], have achieved a fast and high-energy-efficiency trotting gait [7] and a dynamic quadrupedal bounding gait [8].

Along with significant progress in quadrupedal robotic systems, a variety of novel control designs for such kinds of robots have been proposed. A control approach using hierarchical operational space control has been developed based on floating body dynamics [9], [10]. In this research, motion planning is inspired by the self stability of the Spring-Loaded-Inverted-Pendulum (SLIP) model and carried out in conjunction with a foot placement strategy similar to the one introduced in [11]. This planned motion is encoded in the robot by solving inverse dynamics in the form of operational space control. Using this approach, the researchers successfully achieved a dynamic trotting gait with a speed of 0.7 m/sec (1.5 body length/sec) in StarlETH. Another dynamic trotting gait is demonstrated in [12] using the hydraulic robot platform HyQ. Desired trajectories of the robot's foot are calculated employing the algorithm inspired by central patten generator (CPG) and implemented on the robot using feed-forward torques provided by floating-base inverse dynamics with PD control. Currently, the HyQ is able to run with a speed of up to 2.5 m/sec with a off-board power source.

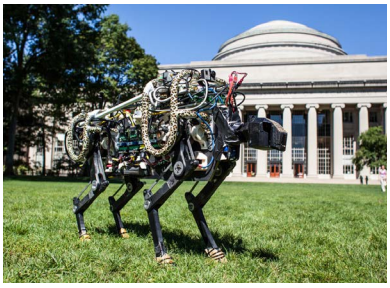

Fig. 1. MIT Cheetah 2 is standing on a grassy field. The robot is untethered, and equipped with on-board batteries and a computer system.

While the researchers achieved a number of successful implementations of their algorithms, most of the algorithms only provided running gaits in a slow speed range ($< Fr = 1.3$). Furthermore, in order to obtain running with different speeds, control parameters have to be re-obtained by hand tuning or iterative and computationally expensive optimization processes [13], [14], [7].

In this paper, we introduce a novel algorithm that allows the MIT Cheetah 2 to run stably over a wide range of speeds from 0 m/sec to 4.5 m/sec without re-tuning or re-optimizing any control parameters. When legged locomotion systems run in high-speed, stance time decreases due to the limited stroke length by the length of the leg. However, the swing duration cannot be decreased to provide consistent accuracy for robots to relocate the swing leg to achieve the desirable configuration in preparation for landing. This is especially important because the attack angle and retraction speed of the swing leg at the moment of landing heavily influence the stability and efficiency of running gaits, as shown in [15], [17]. Drawing on this observation, our approach divides a control problem into two sub-problems: how to manage shorter stance time as running speed increases without reducing swing time, and how to maintain forward running speed while reducing pitch oscillation. As a solution to the problems, a simple impulse planning algorithm is introduced by employing the principle that a system's momentum does not change if the net impulse by external forces is zero. By designing force profiles for vertical and horizontal forces such that the net impulse during one stride is zero, we obtained a periodic orbit with various running speeds. This impulse planning algorithm provides scaled vertical impulse

This work was supported by the Defense Advanced Research Program Agency M3 program

[1]Authors are with the Department of Mechanical Engineering, Massachusetts Institute of Technology, Cambridge, MA, 02139, USA , corresponding email: parkhw at mit.edu

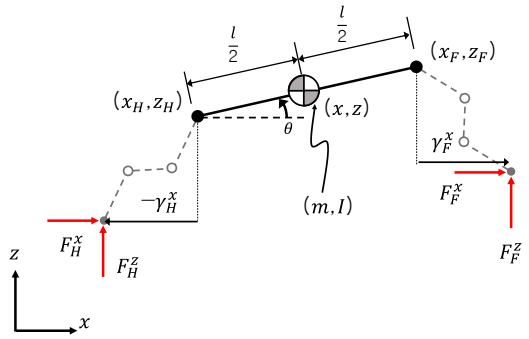

Fig. 2. Simplified Sagittal Plane Model of the MIT Cheetah 2 Robot. The legs are modeled as massless, and the effect of the legs on the body's dynamics are included as forces at the shoulder of the robot similar to [18].

to balance the impulse created by gravity as stance duration decreases. Previously, we mainly addressed this problem in [8]. This impulse planning algorithm also provides horizontal impulse in order to decrease oscillation in pitch while maintaining forward running speed. The proposed algorithm was successfully implemented on the robot utilizing a unique high-bandwidth actuation of the MIT Cheetah 2 [5]. The robot was able to run on a hard treadmill surface as well as a rough and soft grass field without any changes in controller, showing that the proposed algorithm is robust to various ground stiffnesses.

The remainder of the paper is organized as follows: Section II explains a simple but accurate model that describes important dynamic behaviors of the robot. Section III explains the underlying principles of the impulse planning algorithm that allow bounding gaits with different speeds. Section IV details how the controller is implemented on the robot. Section V summarizes the experimental results of the bounding gait of the MIT Cheetah 2. Section VI concludes the paper.

II. Simplified Sagittal Plane Model

A quadruped runner can be modeled as a two-legged sagittal plane model, as shown in Figure 2, because we restrict our attention to the bounding gait where front and hind pairs of the leg act as in sync [19]. The generalized coordinates of the robot are taken as $q := (x, z, \theta)$ where x and z are the horizontal and vertical position of the body's center of mass and θ is the angle of the body. This model assumes massless legs and the effect of the leg on the body's dynamics is included in the horizontal ground reaction forces $F_{F,H}^x$ and vertical ground reaction forces $F_{F,H}^z$ at the foot of the front and hind legs. The equations of motion of the body are shown below.

$$\begin{aligned} m\ddot{x} &= F_F^x + F_H^x \\ m\ddot{z} &= -mg + F_F^z + F_H^z \\ I\ddot{\theta} &= F_F^z\left(\frac{l}{2}\cos\theta + \gamma_F^x\right) + F_H^z\left(-\frac{l}{2}\cos\theta + \gamma_H^x\right) \\ &\quad + F_F^x\left(-\frac{l}{2}\sin\theta + z\right) + F_H^x\left(\frac{l}{2}\sin\theta + z\right) \end{aligned} \tag{1}$$

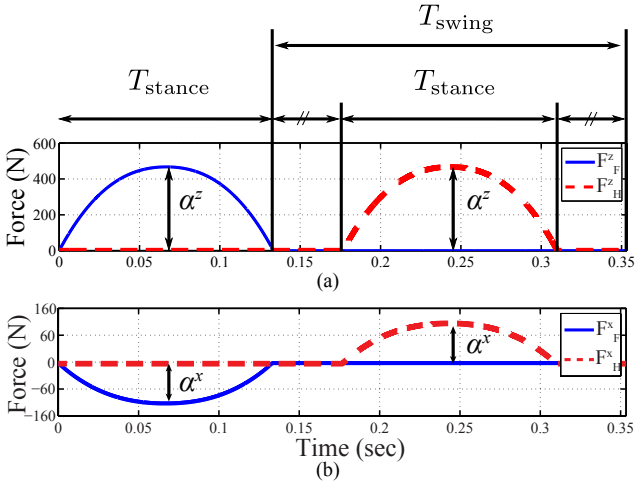

Fig. 3. Force profile when $T_{\text{stance}} = 133$ msec and $T_{\text{swing}} = 220$ msec. Top: vertical force profile. Bottom: horizontal force profile.

The body's mass m and inertia I are 33 kg and 2.9 kg m^2 respectively, length l of the body is 0.7 m, and the center of mass is located in the middle of the body. All the inertial and kinematic parameters are drawn from the CAD model of MIT Cheetah 2 robot. γ_F^x and γ_H^x are the relative horizontal distance from the shoulder to the foot (see Figure 2) and introduced to include the effect of the horizontal change in foot position change relative to the shoulder as the robot runs forward. Provided that the horizontal leg stroke during stance is 0.4 m (the value chosen by considering the length of the leg during the stance 0.5 m) and touch-down and take-off happen in symmetric configurations of the leg, the values of γ_F^x and γ_H^x start with 0.2 m and decrease at the rate of the running speed v during stance.

The model is symmetric in the fore-aft direction, and dynamics in the direction of x and z are decoupled from each other. Therefore, we can assume that the control of the vertical and horizontal directions will be separate problems. This can be clearly seen from the equations of motion above.

III. Periodic Limit Cycle Design using Impulse Planning

If we integrate the first two equations of the dynamic model in (1) with respect to time over an interval $[0, T]$ where 0 is the beginning of the step and T is the end of the step, then the integrated equation becomes,

$$\begin{aligned} m(\dot{x}(T) - \dot{x}(0)) &= \int_0^T (F_F^x + F_H^x)dt \\ m(\dot{z}(T) - \dot{z}(0)) &= -\int_0^T mgdt + \int_0^T (F_F^z + F_H^z)dt \end{aligned} \tag{2}$$

This integrated form of the dynamics clearly depicts the principle that change in linear momentum during the stride shown in the left hand side of the equation equals the net impulse created by total external forces shown in the right hand side of the equation. Therefore, if force profiles for F_F^x, F_H^x, F_F^z and F_H^z are chosen such as to make the net

impulses created by external forces zero as following,

$$\int_0^T (F_F^x + F_H^x)dt = 0 \tag{3}$$

$$-\int_0^T mgdt + \int_0^T (F_F^z + F_H^z)dt = 0, \tag{4}$$

then momentum at the start of step and at the end of the step will be unchanged. Accordingly, the values of $\dot{x}$ and $\dot{z}$ at the start of the gait and at the end of the gait will be same, satisfying the periodicity condition on $\dot{x}$ and $\dot{z}$. Figure 3 shows an example of force profiles that satisfies (3) and (4). Vertical forces are selected to be positive to balance with the impulse created by the gravity $-\int_0^T mgdt$. Horizontal forces of front and hind foot are chosen to be positive and negative to make the impulses created by them cancel each other.

Equation (4) is also used to scale the vertical impulse created by F_F^z and F_H^z as the running speed varies in order to balance the vertical impulse created by gravity. Given that the relative distance in which the robot contacts the ground during the stance is limited by the workspace of the leg, the stance duration should be decreased as the running speed increases. Hence, duty cycle of the bounding gait should decrease accordingly unless the duration of swing decreases significantly. The experimental data of dog running show that the stance time decreases as the running speed increases, whereas the swing time remains constant over a wide range of speeds [20], [21]. Following this observation from biology, swing time is chosen to be constant as speed varies in this paper. Then, the duty cycle decreases as running speed increases. As duty cycle decreases, a greater yet proper amount of vertical force must be provided to make the body jump up off the ground within decreased stance time while also providing enough swing time for leg protraction and retraction.

Horizontal force is selected to decrease pitch oscillation. We can make the direction of force at the front leg F_F and hind leg F_H point toward the center of mass by choosing horizontal force F_F^x to be negative and F_H^x as to be positive as shown in Figure 3. By making the forces point toward the center of mass, we can reduce the moment arm of the forces with respect to the center of mass. This reduced moment arm decreases torque acting upon the body, thereby decreasing motions in pitch. We set the magnitude of F_F^x and F_H^x identical to satisfy (3).

In this rest of section, we will provide the details of how to choose the force profiles.

A. Vertical Force Profiles - Duty Cycle Modulation via Vertical Impulse Scaling

This section presents the selection of vertical force profiles which not only make net vertical impulse zero but also modulate the duty cycle of the running gait to achieve variable duty-cycle running.

1) Selection of Force Profile: The vertical forces F_F^z and F_H^z are chosen as time-dependent profiles shown in Figure 3(a), which are parametrized as,

$$F_i^z = h(\alpha_i^z, s_i, T_{\text{stance}}, T_{\text{swing}}), \text{ for } i = F, H, \tag{5}$$

where α^z is the scalar value representing the magnitude of the force profile, as depicted in Figure 3(a), T_{stance} is the duration of the stance where the legs affect the dynamics of the body by the forces at the shoulder, and T_{swing} is the duration of the swing where the leg is not touching the ground. Because horizontal leg stroke during the stance is set to 0.4 m, T_{stance} can be calculated as $0.4/v$. s_i is the normalized time representing percentage of the stance phase completed and given by,

$$s_i = \begin{cases} \frac{t - t_i^{\min}}{t_i^{\max} - t_i^{\min}}, & \text{for } 0 \le s_i \le 1 \\ s_i = 0, & \text{for } s_i < 0 \\ s_i = 1, & \text{for } s_i > 1 \end{cases} \tag{6}$$

For the sake of brevity, the parameters $t_i^{\min}$ and $t_i^{\max}$ are selected so that stance phase of the front legs starts at the beginning of the gait and stance phase of the hind legs starts in the middle of the gait as illustrated in Figure 3.

$$t_F^{\min} = 0, t_F^{\max} = T_{\text{stance}}, t_H^{\min} = \frac{1}{2}T, t_H^{\max} = \frac{1}{2}T + T_{\text{stance}}$$

The force profile of the front leg is made up of 3^{rd}-order Bézier polynomials, where the Bézier coefficients are given by,

$$\beta^z = \begin{cases} \alpha^z \,[0.0\ 0.8\ 1.0\ 1.0] & \text{for } s_i \le s_{\text{peak}} \\ \alpha^z \,[1.0\ 1.0\ 0.8\ 0.0] & \text{for } s_i > s_{\text{peak}} \end{cases} \tag{7}$$

where, s_{peak} is the parameter to change the position of the peak. Here, we set $s_{\text{peak}} = 0.5$ (the peak occurs in the middle of stance phase), but will adjust this value to $s_{\text{peak}} = 0.3$ during the running experiment explained in Section V. The coefficients in (7) are chosen to ensure smooth continuity between the two Bézier polynomials, and for easy scaling of the force profile. Additional simplification can be done by assuming the same scalar value α^z for the front and hind legs.

Duration of the swing phase T_{swing} was chosen to be 0.22 sec which is taken from the swing duration of Cheetah and Greyhound during galloping [20], [21].

2) Modulation of Stance Duration: From the previous section, we can see that only two remaining parameters remain undefined for describing the vertical force profile, which are the duration of stance T_{stance} and the magnitude of the force profile α^z. Here, we will draw the relation between those two parameters using (4) which is rewritten here as,

$$\int_0^T (F_F^z + F_H^z)dt = \int_0^T mgdt \tag{8}$$

where $T := T_{\text{stance}} + T_{\text{swing}}$ is the total duration of one step. Because the area under the Bézier curve can be simply calculated by averaging the Bézier coefficients multiplied by the length of duration, (8) is rewritten by,

$$2\alpha^z c T_{stance} = mgT, \tag{9}$$

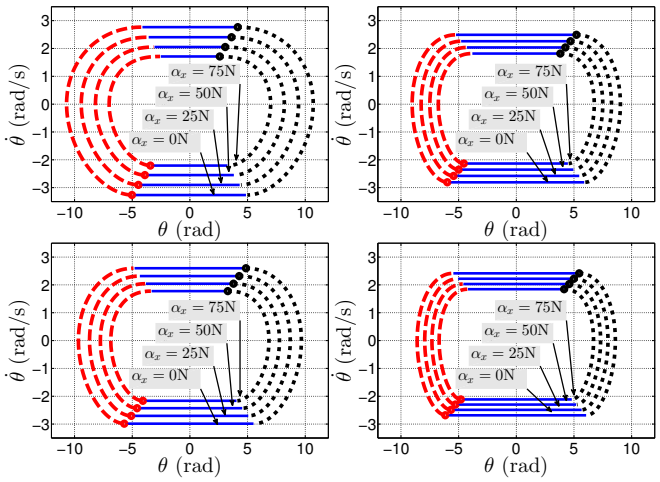

Fig. 4. Phase plot of body pitch angle θ for periodic orbit for various values of v and α_x. Red dashed line represents the front leg stance phase. Black dotted line represents the hind leg stance phase. Start of the stance phase is represented by the circle. Blue line represents the airborne durations. Top Left: $v = 3.5$ m/sec Bottom Left: $v = 4.5$ m/sec Top Right: $v = 5.5$ m/sec Bottom Right: $v = 6.5$ m/sec

where $c = \mathrm{E}\left[\frac{1}{2}\left[0.0\ 0.8\ 1.0\ 1.0\right] + \frac{1}{2}\left[1.0\ 1.0\ 0.8\ 0.0\right]\right]$ is the unit area under the force profile when $\alpha^z = 1$ and $T_{\text{stance}} = 1$. From (9), α^z is given by,

$$\alpha^z = \frac{mgT}{2cT_{\text{stance}}} \tag{10}$$

Equation (10) will be used to calculate the magnitude of force profile α^z when T_{stance} is given. Now, all the parameters associated with the vertical force profile are defined given the value of T_{stance}. Figure 3(a) shows an example of force profile when $T_{\text{stance}} = 0.133$ sec.

B. Horizontal Force Profiles - Decreasing Pitch Oscillation

The horizontal forces F_F^x and F_H^x are chosen to be time-dependent profiles as shown in Figure 3(b), which are parametrized as,

$$F_i^x = h(\alpha^x, s_i, T_{\text{stance}}, T_{\text{swing}}),\ \text{for}\ i = F, H, \tag{11}$$

where, α^x is the magnitude of the force profile. Horizontal Force Profiles are also selected as 3rd-order Bézier polynomials, and the Bézier coefficients of the front leg are given by,

$$\beta_f^x = \begin{cases} -\alpha^x\left[0.0\ 0.8\ 1.0\ 1.0\right] & \text{for}\ s_i \le 0.5 \\ -\alpha^x\left[1.0\ 1.0\ 0.8\ 0.0\right] & \text{for}\ s_i > 0.5 \end{cases} \tag{12}$$

The Bézier coefficients of the hind leg are given by,

$$\beta_h^x = \begin{cases} \alpha^x\left[0.0\ 0.8\ 1.0\ 1.0\right] & \text{for}\ s_i \le 0.5 \\ \alpha^x\left[1.0\ 1.0\ 0.8\ 0.0\right] & \text{for}\ s_i > 0.5 \end{cases} \tag{13}$$

Because the areas of front and hind leg profiles cancel each other as shown in Figure 3(b), (3) is satisfied.

In the next section, we will search for periodic orbits where the vertical force profiles with various values of T_{stance} and horizontal force profiles with various values of α^x are applied to the simplified model.

C. Periodic Limit Cycle

Periodic orbits have been found by searching for fixed points of the following Poincaré return map, as defined by $\mathcal{P} : \{(x,t)\,|t = 0\} \to \{(x,t)\,|t = T\}$[1],

$$x^* = \mathcal{P}(x^*, T_{\text{stance}}, \alpha^x), \tag{14}$$

A large number of fixed points have been computed numerically for $T_{\text{stance}} \in [0.0571\ 0.133]$ sec (corresponds to the running speed v from 7 m/sec to 3 m/sec) and $\alpha^x \in [0\ 200]$ N using MATLAB's `fmincon` function. Figure 4 shows obtained periodic orbit for $T_{\text{stance}} = 114, 89, 73, 62$ msec ($v = 3.5, 4.5, 5.5, 6.5$ m/sec) and $\alpha^x = 0, 25, 50, 75$ N. It is observed that larger values of α^x provide periodic orbits with smaller pitch oscillation. However, the value cannot be increased excessively because of the friction cone constraints in the foot-ground interface. Therefore, we selected 50 N as the value of α^x to make the friction coefficient less than 0.2. We used the same value of α^x over the range of stance duration $T_{\text{stance}} \in [0.0571\ 0.133]$ sec ($v \in [3\ 7]$ m/sec) because, as observed in Figure 4, the effect of α^x on the pitch oscillation does not vary significantly as speed changes.

Linearizing (14) about the fixed point x^* corresponding to the periodic orbit results in a discrete linear system, which is given by,

$$\Delta x[i+1] = A\Delta x[i], \tag{15}$$

where $\Delta x = x - x^*$, and

$$A = \left.\frac{\partial \mathcal{P}}{\partial x}\right|_{x=x^*}. \tag{16}$$

Calculation of the largest eigenvalue of matrices A corresponding to the $T_{\text{stance}} \in [0.0571\ 0.133]$ sec and $\alpha^x \in [0\ 200]$ N revealed that the obtained periodic orbits are unstable.

D. Feedback Control

In order to obtain locally stabilized periodic orbits, we introduce a simple feedback controller during the stance phase. The following simple PD control is added onto the vertical force profile F_i^z obtained in (5),

$$F_{fb}^z = -k_p^z(z_i - z_d) - k_d^z(\dot{z}_i),\ \text{for}\ i = \mathrm{F}, \mathrm{H}, \tag{17}$$

where, z_F and z_H are the height of the front and hind shoulders, k_p^z is the stiffness, k_d^z is the damping, z_d is the set point value for the height of the shoulders which is set to 0.5 m. We could use a time-dependent trajectory for the set point obtained from the corresponding periodic orbit to exactly track the open-loop trajectory, but this causes different sets of trajectories for different values of T_{stance} and α^x. Because our focus is to obtain a stable periodic orbit for various T_{stance} rather than to follow exact trajectories, a single set point value for all cases of T_{stance} and α^x is sought after in this paper.

[1]Application of a time-dependent force profile creates a non-autonomous dynamic system, resulting in a Poincaré section with states x and time t [22].

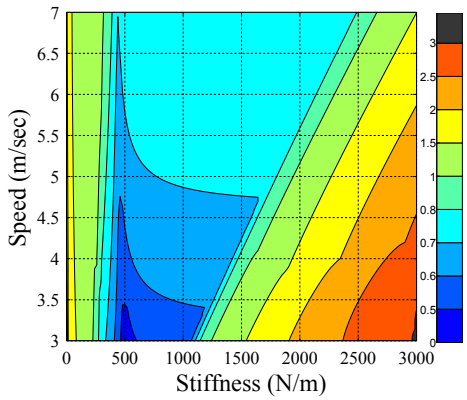

Fig. 5. The largest eigenvalues of linearized Poincaré map for $k_{p,z} \in [0, 3000]$ and $v \in [3, 7]$m/sec.

The following simple feedback is added onto the horizontal force profile F_i^x to regulate the running speed.

$$F_{fb}^x = -k_d^x(\dot{x}_i - v), \text{ for } i = \mathrm{F}, \mathrm{H} \tag{18}$$

where, k_d^z is the damping, and v is the desired running speed. Damping $k_{d,x}$ and $k_{d,z}$ are chosen to be 40 Ns/m and 120 Ns/m respectively for the simulation. These are the maximum values possible before the real-hardware becomes unstable due to the noise caused by the numerical differentiation of the encoder signal.

Because the feedback is added onto the original force profile and influences the dynamics of the system, the behavior of the system will be changed accordingly. Therefore, new fixed points should be calculated numerically. A large number of fixed points have been computed for different values of $T_{\text{stance}} \in [0.0571, 0.133]$ sec and $k_p^z \in [0, 3000]$.

$$\bar{x}^* = \mathcal{P}(\bar{x}^*, k_p^z, T_{\text{stance}}). \tag{19}$$

The eigenvalues of the linearized Poincaré map A for $k_{p,z} \in [0, 3000]$ and $T_{\text{stance}} \in [0.0571, 0.133]$ are calculated, and the largest eigenvalues are plotted in Figure 5. The result shows that addition of the feedback yields a stable periodic orbit for a wide range of the value of k_p^z for all $T_{\text{stance}} \in [0.0571, 0.133]$. k_p^z is selected as 500 N/m because the value provides a stable periodic orbit for all $T_{\text{stance}} \in [0.0571, 0.133]$. We would like to note that this value of stiffness 500 N/m is very small and around 10% of the stiffness value used in the previous trotting experiments of MIT Cheetah where only an impedance controller was used [7], meaning designed force profiles will play an important role in control design to create bounding motions.

IV. Implementation of the Algorithm

This section presents the implementation of the algorithm on the real robot hardware. Force profiles F_i, where $i = F, H$, obtained from Section III-A are implemented in the robot through the torques of the motors in the legs of the MIT Cheetah 2. As shown in Figure 6(a), each leg of the MIT Cheetah 2 consists of three links from the shoulder joint, and the motions of first and last link from the shoulder are kinematically tied to be parallel to each other, resulting

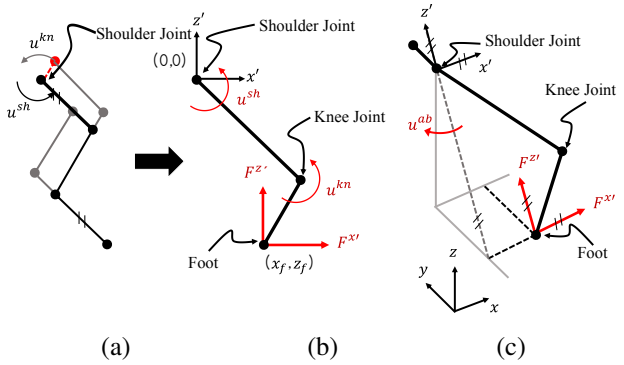

Fig. 6. (a) MIT Cheetah's leg consisting of three links. First and third links are kept in parallel each other by parallelogram mechanism. (b) Two links kinematic conversion of original link structure. Using the torques u^{sh} and u^{kn} at shoulder and knee joints, forces $F^{x'}$ and $F^{z'}$ are generated. (c) An actuator to create ab/adduction torque u^{ab} for each leg.

in two degree of freedom links. The first actuator torque u^{sh} rotates the link represented by the thick solid black line, providing rotation of all three links relative to the body. The second actuator torque u^{kn} rotates the link represented by the dashed red line, yielding rotation of the second link while the first and third links are kept in parallel. Because the first and third links are parallel, the original link structure can be kinematically converted to a mechanism with only two links shown in Figure 6(b). In addition to actuators for the knee and shoulder angles, there is one more actuator to create ab/adduction torque u^{ab} for each leg (see Figure 6(c)).

A. Application of Force Profile and Feedback

In this section, we obtain a static force/torque relationship to create horizontal, lateral, and vertical forces, and the rolling torque (F^x, F^y, F^z, τ^x in Figure 7) using the joint torques in each pair of legs. We could calculate the exact required actuator torques to provide the desired horizontal and vertical direction ground reaction forces by solving the inverse dynamics, but a static force/torque relationship is only considered in this paper instead. This approximation in calculating the control inputs is reasonable because the robot's leg is relatively light compared to the body (less than

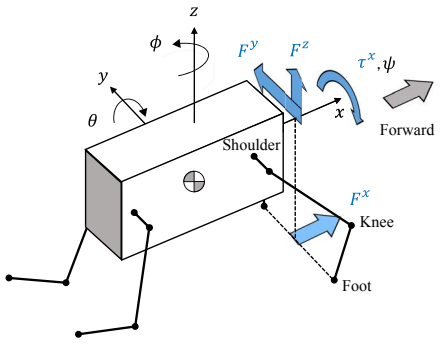

Fig. 7. Coordinates system and control forces of MIT Cheetah 2. ψ, θ, and ϕ are roll, pitch, and yaw angles representing rotations about x, y, and z axis, respectively. The horizontal force F^x, lateral force F^y, vertical force F^z, and rolling torque τ^x are generated using actuator torques of each pair of the legs (see Figure 6 and 8).

10% of body mass).

The procedure for obtaining the relationship is two-fold. Figure 8 depicts this procedure. In the first step, an auxiliary planar coordinate system $x'z'_L$ rotated from the xz coordinate system with ab/adduction angle q_L^{ab} is attached on the shoulder joint (see Figure 8(a)). In this planar coordinate system, we can obtain a mapping of the forces $F_L^{x'}$ and $F_L^{z'}$ at the left foot shown in Figure 8 to the torques u_L^{sh} and u_L^{kn} which is given by,

$$\begin{bmatrix} u_L^{sh} \\ u_L^{kn} \end{bmatrix} = J_{x'z'_L}^T \begin{bmatrix} F_L^{x'} \\ F_L^{z'} \end{bmatrix}, \tag{20}$$

where, $J_{x'z'_L}$ is the manipulator Jacobian obtained by taking the partial derivative of the position of the foot relative to the shoulder in $x'z'_L$ coordinates with respect to the knee and shoulder joint angles. For the right leg, the same procedure is followed. Then, the horizontal force F^x is just the summation of left and right horizontal forces $F_L^{x'}$ and $F_R^{x'}$ as shown in Figure 8(a). In order to avoid unnecessary yaw torque, $F_L^{x'}$ and $F_R^{x'}$ are chosen to be the same, thereby obtaining,

$$F_L^{x'} = F_R^{x'} = \frac{1}{2}F^x. \tag{21}$$

In the second step, we obtain a linear operator J_{frt}^T which maps a vector $F_{\text{frt}} := [F^y \ F^z \ \tau^x]^T$ to a vector $u_{\text{frt}} := [F_L^{z'} \ F_R^{z'} \ u_L^{ab} \ u_R^{ab}]^T$ (see Figure 8(b)) as following,

$$u_{\text{frt}} = J_{\text{frt}}^T F_{\text{frt}} \tag{22}$$

To systematically obtain the mapping, we define the generalized coordinates of floating base frontal dynamics as,

$$q_{\text{frt}} := [q_{\text{float}}^T, z_L, z_R, q_L^{ab}, q_R^{ab}]^T \in \mathbb{R}^{7\times 1} \tag{23}$$

where, $q_{\text{float}} = [y_b, z_b, \psi]^T$ and y_b and z_b are the position of the body, ψ is the roll angle, z_L and z_R are the length of the left and right legs in frontal plane, q_L^{ab} and q_R^{ab} are ab/adduction angles of left and right legs (see Figure 8(b)). Because two legs are contacting the ground and forming a closed loop structure, we have to take into account the constraints that the feet are not moving with respect to the ground. Let $p_f \in \mathbb{R}^{4\times 1}$ be the vector which has the elements of horizontal and vertical foot position of the left and right legs in the frontal plane. Then, the constraints can be written as,

$$\delta p_f = \frac{\partial p_f}{\partial q_{\text{frt}}} \delta q_{\text{frt}} \equiv 0. \tag{24}$$

Because of this constraint on the foot, the system has only $7 - \text{rank}\left(\frac{\partial p_f}{\partial q_{\text{frt}}}\right) = 3$ degrees of freedom and its dynamics can hence be fully described using minimal coordinates $q_{\text{frt}}^{\text{consist}} \in \mathbb{R}^{3\times 1}$ [10]. The relation between virtual displacements of generalized coordinates δq_{frt} and minimal coordinates $\delta q_{\text{frt}}^{\text{consist}}$ can be obtained by,

$$\delta q_{\text{frt}} = Q \delta q_{\text{frt}}^{\text{consist}} \tag{25}$$

where, $Q \in \mathbb{R}^{7\times 3}$ is the linear operator which satisfies,

$$\frac{\partial p_f}{\partial q_{\text{frt}}} Q = 0 \tag{26}$$

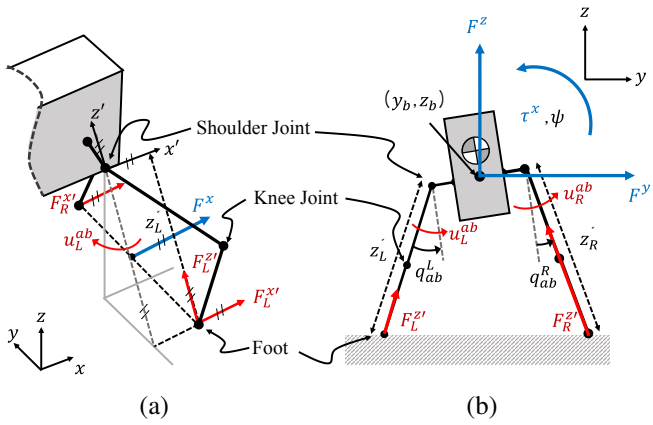

Fig. 8. Generation of the lateral force F^y, vertical force F^z, and rolling torque τ^x using forces $F_L^{z'}$, $F_R^{z'}$ and torques u_L^{ab}, and u_R^{ab} in two legs contacting with the ground. y_b and z_b are the position of the center of the left and right shoulder joints in frontal plane, and ψ is the rolling angle of the body, $q_{L,R}^{ab}$ are ab/adduction angles of the left and right legs.

Now, to obtain J_{frt}^T, the principle of virtual work is used.

$$\left(\frac{\partial q_{\text{float}}}{\partial q_{\text{frt}}}^T F_{\text{frt}}\right)^T \delta q_{\text{frt}} = (B_{\text{frt}} u_{\text{frt}})^T \delta q_{\text{frt}} \tag{27}$$

where, B_{frt} is the matrix which maps actuator torques to generalized torques. Substituting (26) into (27), and taking the transpose yields,

$$(\delta q_{\text{frt}}^{\text{consist}})^T Q^T \frac{\partial q_{\text{float}}}{\partial q_{\text{frt}}}^T F_{\text{frt}} = (\delta q_{\text{frt}}^{\text{consist}})^T Q^T B_{\text{frt}} u_{\text{frt}} \tag{28}$$

Now, we can obtain J_{frt}^T by rewriting (28),

$$u_{\text{frt}} = \left(Q^T B_{\text{frt}}\right)^+ Q^T \frac{\partial q_{\text{float}}}{\partial q_{\text{frt}}}^T F_{\text{frt}} = J_{\text{frt}}^T F_{\text{frt}} \tag{29}$$

where, M^+ is a pseudo-inverse of matrix M. Finally, using (20), (21), and (29), the joint torques $u_L^{sh}, u_R^{sh}, u_L^{kn}, u_R^{kn}, u_L^{ab}, u_R^{ab}$ which generate F^x, F^y, F^z, τ^x can be calculated.

To implement the algorithm we obtained in Section III, which combines the force profile and feedback with low gain, F^z and F^x are selected as,

$$\begin{aligned} F^x &= F_i^x - k_{p,x}(x - x_d) - k_{d,x}(\dot{x} - \dot{x}_d) \\ F^z &= F_i^z - k_{p,z}(z - z_d) - k_{d,z}\dot{z}, \ \text{for } i = F, H \end{aligned} \tag{30}$$

where, x_d is the desired trajectory for the horizontal motion to produce a leg swing motion with the desired speed v, and z_d is the desired shoulder height which is chosen as $0.48\ m$. To regulate the lateral sway and rolling motion of the body, F^y and τ^x are chosen as,

$$\begin{aligned} F_y &= -k_{p,y} y_b - k_{d,y}\dot{y_b} \\ \tau_x &= -k_{p,\psi}\psi - k_{d,\psi}\dot{\psi} \end{aligned} \tag{31}$$

To regulate yaw motion, the following feedback is calculated,

$$F_i^{y,\phi} = G_{\text{sign}}\left(-k_{p,\phi}(\phi - \phi_d) - k_{d,\phi}\dot{\phi}\right) \tag{32}$$

where, ϕ_d is the desired yaw angle, and $G_{\text{sign}} = 1$ and -1 for front leg and hind leg. This feedback is added to the force F_y in (31).

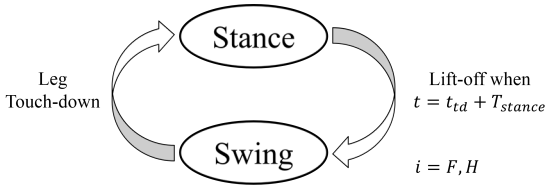

Fig. 9. Stance Machine for front and hind legs.

B. Swing Phase Control and Detection of Impact with the Ground

During the swing phase, the corresponding legs are controlled to follow a desired trajectory. The desired trajectory is designed to perform the following necessary motions sequentially during the swing: retracting the leg backward for the clearance of the leg from the ground, throwing the retracted leg forward quickly, and retracting the leg rearward to prepare for touchdown. A simple feedback control based on a Cartesian-computed torque controller [23] is used to track the designed trajectories. Impact with the ground is detected by proprioception, observing the force in the z direction created by joint actuators. Required nominal z direction force to create the desired swing motion is logged from prior swing leg motion experiments during which the robot is hanging in the air. This is used to create a table of nominal forces to reduce incidents of false positives. In the bounding experiment, if the z direction force during swing phase is larger than this logged nominal force by some margin, this additional force is assumed to be caused by the impact with the ground and touchdown is declared. However, this could lead to a delay in the detection of ground impact during bounding.

C. Finite State Machine

The last step of the implementation process is to introduce a state machine to manage the transition between stance and swing phase for each leg. Two independent finite state machines for each pair of front and hind legs is proposed while the transition of a pair of left and right legs occurs together. Timing synchronization between the front pair of legs and hind pair of legs is done by adjusting the duration of the stance T_{stance} and swing T_{swing} according to the error measured at the transition between phases. The state machine is illustrated in Figure 9. The transition from swing to stance occurs when the leg strikes the ground. Transition from stance to swing takes place when time reaches $T_{\text{stance}} + t_{td}$ where t_{td} is the touchdown time when the leg strikes the ground.

V. Experiments

This section documents the experimental results of the controller. The experiment starts with the robot standing on four legs until an operator initiates bounding. At the first step, the time-dependent force profile depicted in Figure 3 is applied, and once the stance phase of the first step is finished (the legs are airborne), the finite state machine for each pair of legs starts. We introduce a scaling parameter $\lambda \in [0\ 1]$ and multiply it by x_d in (30) and the desired horizontal

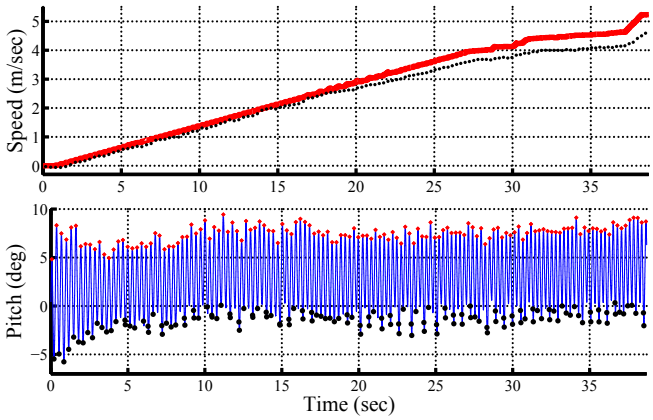

Fig. 10. Top: Measured running speed (black dot) and commanded speed v_{cmd} (red solid line). Measured running speed is obtained by averaging the horizontal speed of the shoulder with respect to the foot during the stance at each step. Bottom: Pitch angle in degrees. Maximum and minimum values of pitch at each step are shown in red diamonds and black dots, respectively.

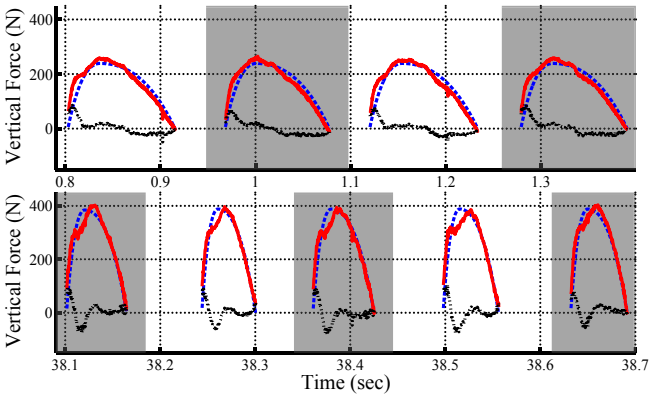

Fig. 11. Vertical Forces applied at the foot due to the force profile (dashed blue), feedback (dotted black), and a combination of both (solid red). White and grey region indicate vertical forces at the front legs and hind legs, respectively. Top: $v = 3.6\text{m/sec}$ and $\lambda = 0.02$. Bottom: $v = 6.9\text{m/sec}$ and $\lambda = 0.76$.

trajectory of the swing phase to scale horizontal movement. By multiplying λ, the commanded speed becomes $v_{\text{cmd}} = \lambda v$. Therefore, when $\lambda = 0$, the leg only moves in the vertical direction so the robot bounds only vertically, and when $\lambda = 1$, the leg moves with the full horizontal stroke length of 0.4 m thereby providing the bounding with the desired speed v.

The experiment starts with $\lambda = 0$ and $v = 3.5$ m/sec, and the values of λ and v are gradually increased by the operator to reach faster speeds. During the experiment, the MIT Cheetah 2 successfully increases its speed from 0 m/sec to 4.5 m/sec stably (see Figure 10 top) while pitch dynamics are mostly bounded between -5 deg and 8 deg (see Figure 10 bottom) as predicted by the simulation (see Figure 4). The top speed was 4.5 m/sec obtained by setting $v = 6.9$ m/sec and $\lambda = 0.76$. However, there is a noticeable error between the commanded speed v_{cmd} and robot's running speed when the robot runs fast. This could be due to the ground impact loss which increases as the running speed increases. An additional algorithm is required to compensate impact loss for high-speed running.

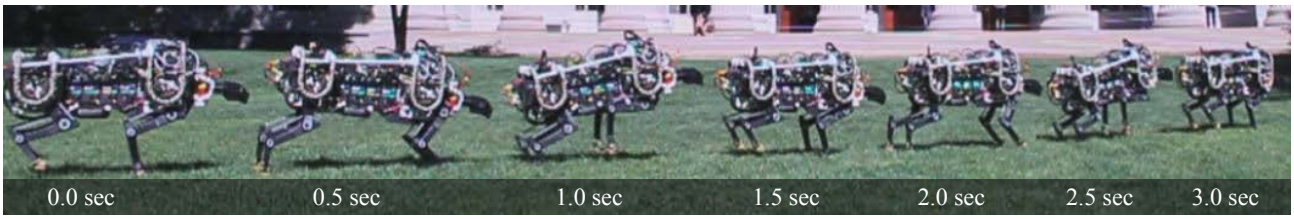

Fig. 12. Snapshots of the running experiment on a grass field.

Figure 11 depicts the vertical force applied at the front (white region) and hind (grey region) leg with $v = 3.6\ \mathrm{m/sec}$ and $v = 6.9\ \mathrm{m/sec}$ (on the bottom). It is observed that feedback (dotted black line) is significantly smaller than the predefined force profile (dashed blue line), showing that the predefined force profile plays a major role in providing the bounding gait with the desired duty ratio.

The control algorithm was further tested to make the MIT Cheetah 2 run on a grass field. Without changing any control parameters, a stable dynamic untethered running was also successfully achieved on the soft grassy field. Figure 12 depicts snapshots of bounding on the grassy field at the intervals of 0.5 sec.

VI. Conclusion

We have successfully demonstrated stable quadruped bounding gaits over speeds ranging from $0\ \mathrm{m/sec}$ to $4.5\ \mathrm{m/sec}$. A prescribed vertical and horizontal force profile is combined with a low gain PD control on the height of shoulders and feedback on running speed, providing stable quadruped bounding in simulation. Next, scaling of vertical impulse to balance with the vertical impulse due to gravity yields multiple periodic orbits with a wide selection of stance durations. The horizontal force profile is chosen to decrease oscillations in pitch while making net horizontal impulse zero. The proposed controller has been successfully validated in experiments on the MIT Cheetah 2, achieving stable untethered high-speed 3D running over a wide range of speed without re-tuning or re-optimizing the control parameters. During 4.5m/s bounding, the recorded power consumption from the battery is about $700\ \mathrm{W}$, corresponding to a cost of transport of 0.5. In near future, we will test the speed limit as well as different gait

References

[1] M. Raibert, K. Blankespoor, G. Nelson, R. Playter, and the BigDog Team, "Bigdog, the rough-terrain quadruped robot," in *Proceedings of the 17th World Congress*, 2008, pp. 10 823–10 825.

[2] Boston Dynamics. (2012) Cheetah robot runs 28.3 mph; a bit faster than usain bolt. Youtube Video. [Online]. Available: http://youtu.be/chPanW0QWhA

[3] C. Gehring, S. Coros, M. Hutter, M. Bloesch, M. Hoepflinger, and R. Siegwart, "Control of dynamic gaits for a quadrupedal robot," in *Robotics and Automation (ICRA), 2013 IEEE International Conference on*, May 2013, pp. 3287–3292.

[4] C. Semini, N. G. Tsagarakis, E. Guglielmino, M. Focchi, F. Cannella, and D. G. Caldwell, "Design of HyQ: a hydraulically and electrically actuated quadruped robot," *Proceedings of the Institution of Mechanical Engineers, Part I: Journal of Systems and Control Engineering*, vol. 225, no. 6, pp. 831–849, 2011.

[5] S. Seok, A. Wang, D. Otten, and S. Kim, "Actuator design for high force proprioceptive control in fast legged locomotion," in *IEEE/RSJ International Conference on Intelligent Robots and Systems*, 2012, pp. 1970–1975.

[6] S. Seok, A. Wang, M. Y. Chuah, D. Otten, J. Lang, and S. Kim, "Design principles for highly efficient quadrupeds and implementation on the mit cheetah robot," in *IEEE International Conference on Robotics and Automation*, 2013, to Appear.

[7] D. J. Hyun, S. Seok, J. Lee, and S. Kim, "High speed trot-running: Implementation of a hierarchical controller using proprioceptive impedance control on the MIT cheetah," 2014.

[8] H.-W. Park, M. Y. Chuah, and S. Kim, "Quadruped bounding control with variable duty cycle via vertical impulse scaling," in *Intelligent Robots and Systems (IROS), 2014 IEEE/RSJ International Conference on*, Sep 2014.

[9] M. Hutter, H. Sommer, C. Gehring, M. Hoepflinger, M. Bloesch, and R. Siegwart, "Quadrupedal locomotion using hierarchical operational space control," *The International Journal of Robotics Research*, 2014.

[10] M. Hutter, "StarlETH & co.- design and control of legged robots with compliant actuation," Ph.D. dissertation, ETH ZURICH, 2013.

[11] M. H. Raibert, *Legged Robots that Balance*. Cambridge, MA: MIT Press, 1986.

[12] V. Barasuol, J. Buchli, C. Semini, M. Frigerio, E. de Pieri, and D. Caldwell, "A reactive controller framework for quadrupedal locomotion on challenging terrain," in *Robotics and Automation (ICRA), 2013 IEEE International Conference on*, May 2013, pp. 2554–2561.

[13] S. Coros, A. Karpathy, B. Jones, L. Reveret, and M. van de Panne, "Locomotion skills for simulated quadrupeds," *ACM Trans. Graph.*, vol. 30, no. 4, pp. 59:1–59:12, July 2011.

[14] H. M. Herr and T. A. McMahon, "A galloping horse model," *The International Journal of Robotics Research*, vol. 20, no. 1, pp. 26–37, 2001.

[15] M. Haberland, J. Karssen, and M. W. S. Kim, "The effect of swing leg retraction on running energy efficiency," in *IEEE/RSJ International Conference on Intelligent Robots and Systems*, Sep. 2011, pp. 3957–3962.

[16] J. Karssen, M. Haberland, M. Wisse, and S. Kim, "The optimal swing-leg retraction rate for running," in *IEEE International Conference on Robotics and Automation*, May. 2011, pp. 4000–4006.

[17] M. Wisse, A. L. Schwab, R. Q. van der Linde, and F. C. T. van der Helm, "How to keep from falling forward: Elementary swing leg action for passive dynamic walkers," *IEEE Transactions on Robotics*, vol. 21, no. 3, pp. 393–401, June 2005.

[18] A. Valenzuela and S. Kim, "Optimally scaled hip-force planning: A control approach for quadrupedal running," in *Robotics and Automation (ICRA), 2012 IEEE International Conference on*, May 2012, pp. 1901–1907.

[19] M. H. Raibert, "Trotting, pacing and bounding by a quadruped robot," *Journal of Biomechanics*, vol. 23, Supplement 1, no. 0, pp. 79 – 98, 1990, international Society of Biomechanics.

[20] L. D. Maes, M. Herbin, R. Hackert, V. L. Bels, and A. Abourachid, "Steady locomotion in dogs: temporal and associated spatial coordination patterns and the effect of speed," *Journal of Experimental Biology*, vol. 211, no. 1, pp. 138–149, 2008.

[21] P. E. Hudson, S. A. Corr, and A. M. Wilson, "High speed galloping in the cheetah (acinonyx jubatus) and the racing greyhound (canis familiaris): spatio-temporal and kinetic characteristics," *Journal of Experimental Biology*, vol. 215, no. 1, pp. 2425–2434, 2012.

[22] T. S. Parker and L. O. Chua, *Practical numerical algorithms for chaotic systems*. Springer New York, 1989.

[23] R. Murray, Z. Li, S. Sastry, and S. Sastry, *A Mathematical Introduction to Robotic Manipulation*. Taylor & Francis, 1994.